Article

Simultaneous Assessment of Reactive Oxygen Species and Radiosensitization of Brain Cancer Cells using Nanoparticle Spectroscopy

Honour Djam [1], Harrison Kramer[2], Caleb Thiegs[1], Anne Hubbard[1], Yohan Walter[1], Michael Merrick[1], Michael Mimlitz[1], Catherine Weeder[2], Haris Akhter[2], Megha Jacob[2], Gargee Khaparde[2], Ashley Abraham[2], Joe Bamesberger[3], and Andrew Ekpenyong[1,*]

[1] Department of Physics, Creighton University, Omaha, USA; honourdjam@creighton.edu (H.D.); calebthiegs@creighton.edu (C.T.); annehubbard1@creighton.edu (A.H.); yohanwalter@creighton.edu (Y.W.); michaelmerrick@creighton.edu (M.M.); michaelmimlitz@creighton.edu (M.J.M.);
[2] Department of Biology, Creighton University, Omaha, USA; harrykramer@creighton.edu (H.K.); catherineweeder@creighton.edu (C.W.); harisakhter@creighton.edu (H.A.); meghajacob@creighton.edu (M.J.); gargeekhaparde@creighton.edu (G.K.); ashleyabraham@creighton.edu (A.A.)
[3] HCB Pre-Health Science, Creighton University, Omaha, USA; joebamesberger@creighton.edu (J.B.)
* Correspondence: andrewekpenyong@creighton.edu; Tel.: +14022802208.

Abstract: Nanoparticle-mediated radiation therapy (NPRT) is an emerging modality for radiosensitization of highly resistant cancers such as brain cancers. This is due to the ability of specific nanoparticles (NPs) to increase physical dose deposition and subsequent direct damage to cells and DNA within their local vicinity, through enhanced generation of reactive oxygen species, ROS. Here, we report the successful use of PEGylated (biocompatible) core-shell quantum dots (QDs) and carbon quantum dots (CQDs) to simultaneously enhance and assess ROS generation while radiosensitizing highly radioresistant brain cancer cell lines: T98G and U87 Glioblastoma cells. Relative peak fluorescence intensity ratio calculations and average intensity comparisons show highly significant (***$p<0.001$) enhancement of ROS generation, for 5 Gy and 20 Gy irradiation, applied using a Faxitron Cell Irradiator. By quantifying post-radiotherapy cell attachment, proliferation, migration, cell survival and cell death using electric cell-substrate impedance sensing and clonogenic assays, we demonstrate potentially improved *in vitro* radiotherapeutic outcomes for brain cancer cells radiosensitized using PEGylated CdSe/ZnS QDs and CQDs.

Keywords: Glioblastoma; Radioresistance; Radiosensitizer; ROS; Nanoparticle; Radiotherapy

1. Introduction

Despite remarkable advances in imaging modalities, treatment planning algorithms and treatment modalities, cancer is still a significant public health problem and the second leading cause of death worldwide [1]. The National Brain Tumour Society estimates that 700,000 people in the United States are currently living with a primary brain tumour [2], with glioblastoma multiforme (GBM) being the most prevalent and aggressive form of the disease with poor prognosis [3]. GBM remains a major clinical challenge due to its aggressiveness [4] and high radioresistance [5]. It requires a very high dose (> 50 Gy) because of its high radioresistance [6,7] and such high doses lead to ravaging cognitive and somatic side effects on patients [8]. After maximal surgical resection of GBM, the incidence of recurrence at the primary tumor site is greater than 80%, and the median patient survival is just 12.2-18.2 months [9,10]. Hence, there are concerted research efforts at improving the outcomes of radiation therapy for brain cancers, including the evaluation of novel nanoparticle-mediated therapy approaches.

The use of nanoparticles (NPs) as radiosensitizers [11] is the focus of this work. Nanoparticle-mediated radiation therapy (NPRT) has a huge potential to improve treatment outcomes through local dose enhancement and improved radiosensitization of cancer

Preprints (www.preprints.org) | NOT PEER-REVIEWED | Posted: 28 November 2022 doi:10.20944/preprints202211.0486.v1

cells [12]. Through enhanced permeability and cellular retention, functionalized high atomic number, Z, and high electron density NPs are quickly taken up into tumor cells and can selectively via the release of secondary electrons increase the local dose to the tumor. It has been demonstrated in several studies that irradiating cancer cells in the presence of high electron density and high atomic number NPs increases the therapeutic index and the therapeutic window [13-15]. The mechanisms through which high electron density and high Z NPs act as radiosensitizers have been demonstrated [16,17]. They enhance the production of secondary electrons and amplify reactive oxygen species (ROS) generation [18]. They also induce acceleration in the G0/G1 phase and accumulation of cells in the G2/M phase leading to massive cell arrest accompanied by an increase in p53 mutations and decrease in its expression [19], among many other effects on cellular responses. Studies have demonstrated that semiconductor quantum dots such as core-shell CdSe/ZnS [20-22] QDs generate more ROS under irradiation. Interestingly, we showed in our recent work that chemotherapeutic drugs such as doxorubicin and daunorubicin which generate more ROS in cell culture medium also lead to a reduction in the fluorescent intensity of core-shell CdSe/ZnS QDs enabling their use for assessment of ROS during chemotherapy and radiotherapy [23,24]. Here, we report a novel approach with the overall objective of improving radiation therapy outcomes by simultaneously radiosensitizing highly radioresistant brain cancer through enhanced ROS production and quantification of the ROS produced using quantum dots.

2. Materials and Methods

2.1. Spectroscopic Equipment

The fluorescence intensity measurements were made using a custom-built setup (Figure 1) consisting of a specially built -UV cuvette holder for 1 cm pathlength cuvettes coupled with two optical fibers (UV/VIS fiber type) at right angles to each other, one connecting with an Ocean Optics spectrometer (USB 650; Ocean Optics, Winter Park, FL, USA) and the other with a LED (3.3 V, 0.2 A) light source (RadioShack, Omaha, NE, USA). The UV cuvette holder was constructed to create a precise and reproducible cuvette positioning as well as to optimize the light absorption by the medium and the fluorescence of the medium without UV saturation. The LED was connected to an external circuit using a power supply designed to limit the current through it. The signal generated by the spectrometer was analyzed using the OceanView 1.6.7 software to produce a graph of fluorescence intensity versus wavelength [24].

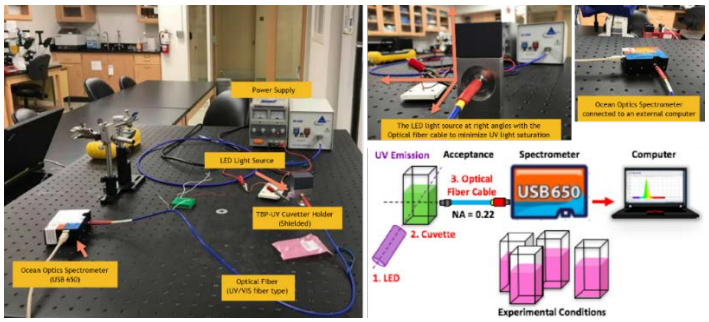

Figure 1. Fluorescence spectroscopy equipment and setup. The colloidal suspension of CdSe/ZnS Core-shell QDs and carbon QDs with cells are illuminated with UV from the LED at room temperature. The fluorescence intensity of the QDs is analyzed by the spectrometer and graphed on a computer using the OceanView v1.6.7 software.

2.2. Chemical Materials and Methods

We used two main NPs, namely, core-shell CdSe/ZnS quantum dots (QSH-540-04 Ocean NanoTech, LLC, and 900244-250UL Sigma Aldrich) and carbon quantum dots (900414-10ml Sigma MKCL6170). The CdSe/ZnS QDs were made biocompatible and functionalized via polyethylene glycol (PEG), an inert polymer which does not interfere with

Preprints (www.preprints.org) | NOT PEER-REVIEWED | Posted: 28 November 2022 doi:10.20944/preprints202211.0486.v1

the optical properties of the QD. We have published details of the protocol for mixing the QDs and CQDs with cells for carrying out spectroscopy [23,24].

2.3. Biological Materials and Methods

We used two human glioblastoma cell lines. The first, T98G, a cell line derived from a 61-year-old Caucasian male, is commonly used in brain cancer research [25]. We purchased the T98G cells from the American Type Culture Collection (ATCC® CRL-1690™), and cultured them following ATCC recommended protocols including the use of EMEM + 10 % (v/v) FBS as the growth medium. The cells were cultured inside an incubator at a temperature of 37°C ± 1°C and 5% ± 1% CO_2 in air atmosphere. The second cell line was U87, a primary human glioblastoma cell line commonly used in brain cancer research [26], which we purchased from ATCC (ATCC® HTB-14™). The U87 cells were cultured using the same medium and conditions as the T98G cells, following ATCC protocols. The average cell density used for the experiments was 1.0 x 10^6 viable cells/ml and only cells at a logarithmic growth phase were used for experiments. This is because the metabolic rate (and hence ROS production) depends on cell density and on cell cycle [24].

2.4. Radiotherapy

To ensure reproducible irradiation that mimics clinical radiotherapy, we used Faxitron's CellRad™ X-ray system (Faxitron Bioptics LLC, Tucson, AZ, USA), a state of art cell irradiator (see SI Figure 1). Equipped with integrated dosimeter and an automatic dose control module, CellRad allows the user to set up target doses and tube currents/voltage to deliver the doses. We used tube voltage and current of 100 kVp and 5 mA respectively for target doses of 5, 10, 20 and 50 Gy with post radiotherapy nanoparticle spectroscopy on the 5 and 20 Gy irradiations. Post-radiotherapy NP spectroscopy was carried out mainly on the 5 Gy and 20 Gy irradiations because of our recent findings about increased migration of cells at those doses [27,28].

2.5. Nanoparticle Spectroscopy

In addition to the details of our nanoparticle spectroscopy [23,24], steps in cell preparation for irradiation and spectroscopy are illustrated in SI Figure 2 and a full experimental workflow is outlined in SI Figure 3, including details such as the incubation of cells with NPs for 1 hour and the completion of all irradiation and spectroscopic measurements within 30 minutes post-NP incubation, since incorporation of NPs by cells is time-dependent. Since the fluorescence intensity of QDs is inversely related to the concentration of ROS in solution, as we [23,24] and others have shown [29], NP radiosensitization studies have computed the percentage change in ROS yield by evaluating the ratio of the peak fluorescent intensity signals of the solution with radiosensitizers to controls without radiosensitizers post-irradiation [27] or by integrating the whole emission spectra to evaluate the relative fluorescence intensity [29-31]. Here, we use peak fluorescence intensity (PFI) ratio in line with several studies [32-34] to assess the relative change in ROS production due to NP radiosensitizers compared to the control. The relative peak fluorescent intensity (RPFI) ratio gives the percentage change in the net peak fluorescent intensity. Unlike the PFI ratio, the RPFI ratio compares only the effect of the addition of NPs in the cell medium with radiation to the effect of radiation alone. The RPFI ratio is obtained thus:

$$\text{Relative PFI Level} = \left| \frac{I_{(\text{Cells+NPs})} - I_{(\text{Cells + NPs + IR})}}{I_{(\text{Cells+NPs + IR})} - I_{(\text{Cells})}} \right| \text{x } 100\%, \quad (1)$$

where $I_{(\text{Cells +NPs+IR})}$ represents the peak intensity of the irradiated cell samples incubated with NPs; $I_{(\text{Cells +NPs})}$ is the intensity of the non-irradiated samples treated with NPs; $I_{(\text{Cells})}$ refers to the peak intensity of the cell samples without irradiation and without NPs, that is, the control samples. For clarity and intuition, the physical significance of the numerator and denominator in Equation 1 are given in Equation (2) thus:

Preprints (www.preprints.org) | NOT PEER-REVIEWED | Posted: 28 November 2022 doi:10.20944/preprints202211.0486.v1

$$\text{Relative PFI Level} = \left|\frac{\text{Net Effect of NPs with IR}}{Net\ Effect\ of\ IR\ only}\right| \text{x } 100\%, \quad (2)$$

The modulus in Equation (1) and its physical cognate, Equation (2), enable the use of absolute values since changes in fluorescent intensity can be either an increase or a decrease.

All experiments were independently repeated at least three times (N1, N2 and N3) and representative plots from these repeats are presented. Each independent repeat (eg, N1) involved taking five acquisitions of fluorescence spectra using the Oceanview v1.6.7 software. These five acquisitions were averaged, and a nonlinear Gaussian fit from the curve fitting suite of OriginPro Graphing and Analysis Software (OrigibLab, Northampton, MA, USA) was used to plot the graphs of average intensity in arbitrary units (a.u.) versus wavelength. Statistical comparisons were done using Analysis of Variance (ANOVA) in OriginLab. Uncertainties are given as ± the standard error of the mean.

2.6. Electric Cell Impedance Sensing (ECIS)

The electric cell-substrate impedance sensing (ECIS) device (Applied BioPhysics Inc, NY, USA) is a commercially available device that provides label-free, real-time, non-invasive analytical and impedance-based technique for quantitative and continuous monitoring of the migratory behavior of adherent cells [35,36]. ECIS has been applied for quantitatively detecting subtle, continuous and dynamic changes in cellular behavior such as adhesion, migration, proliferation and cell death [35,37-39], including the post radiotherapy and post chemotherapy migration of U87 [40] and T98 [27] cells. Here, we have used ECIS similarly to demonstrate the therapeutic impact of radiosensitized GBM cells based on migration and proliferation. SI Figure 4 summarizes how ECIS works, and SI Figure 5 illustrates ECIS results where the time-dependent impedance or resistance serves to quantify proliferation, migration and cell death. An adapted NP-mediated Enhancement Ratio (NER) can be used to quantify the effectiveness of our NPRT. Classically, NER is the ratio of survival fractions without and with NPs for a specific dose [32,34]. For straightforward assessment of the possible radiosensitizing effect of the NPs, we carried out clonogenic assays, which enabled us to obtain survival curves and to make comparisons in view of future NER calculations in the context of more clinically relevant dose-fractionation modalities.

2.7. Clonogenic Assays

We used two colony formation assays, namely, a traditional end-point dye-based manual counting assay called CellMAX™ Clonogenic Assay Kit (BioPioneer, San Diego, USA) and a new automated real-time, label-free and cloud-based live imaging assay, called CytoSMART Omni (CytoSMART Technologies, Eindhove, Netherlands). The CellMAX™ Clonogenic Assay involved fixing the cells, staining and counting. We followed the manufacturers protocol and considered colonies to be made of at least 50 cells.

The CytoSMART Omni is equipped with an automated bright-field microscope with a 10x field objective and a 5 MP CMOS camera that visualizes an entire surface of a cell culture vessel and operates from inside a standard CO_2-incubator. It captures cellular behavior in real time by providing high-quality time-lapse videos for days or weeks at a time. We recorded images every 24 hours, for 14 days or 21 days for each of our experiments and thus have data for colonies formed at any time before the end points of 14 days or 21 days.

3. Results

3.1. CdSe/ZnS spectroscopy with T98G Glioblastoma Cells

Nanoparticle spectroscopy was carried out as described above, following incubation of cells at a density of 1.0×10^6 viable cells/ml with a determined concentration of NPs and

Preprints (www.preprints.org) | NOT PEER-REVIEWED | Posted: 28 November 2022 doi:10.20944/preprints202211.0486.v1

subsequent irradiation. Figure 2 shows representative results of PEGylated CdSe/ZnS QD fluorescence spectroscopy for T98G cells with 0.40 μM QD concentration.

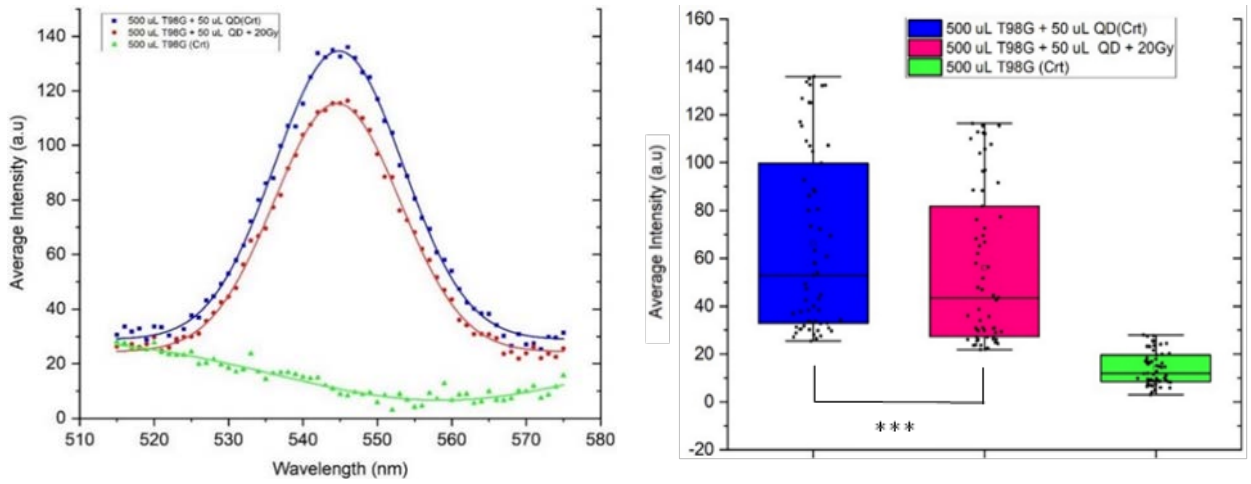

(**a**) (**b**)

Figure 2. QD fluorescence spectra and statistical comparisons for T98G glioblastoma cells. (a). Average intensity plotted as a function of wavelength. T98G cells treated with 0.40 μM core-shell PEGylated CdSe/ZnS QD before 20 Gy irradiation show reduced intensity. (b). Boxplot showing the range, peak, and mean intensities of all three conditions in (a). ANOVA gives a statistically significant (***p<0.001) difference in intensities between 20 Gy irradiated (T98G+QD+20 Gy) and non-irradiated cells (T98G+QD).

Figure 2 is representative of three independently repeated experiments. As expected, the T98G cells without QD which serve as control, show no fluorescence emission. But there is a statistically significant (***p<0.001) reduction in peak intensities between the non-irradiated cells (T98G+QD) and the 20 Gy irradiated (T98G+QD+20 Gy). The reduction in peak intensity is from 136 ± 0.5 a.u to 116.4 ± 0.5 a.u. (Figure 2a,b) with a relative change in peak intensity of 14.4 ± 0.5%. The calculated RPFI due to the NPs is 449.6 ± 4.4%. Thus, irradiating human glioblastoma cells (T98G) incubated with 0.40μM PEG CdSe/ZnS core-shell quantum dots led to a statistically significant (***p<0.001) optical quenching of 14.4 ± 0.5% in the QD fluorescence intensity. This illustrates the increased generation of ROS in the 20 Gy irradiated cells following incubation with QDs.

SI Figure 6 shows a representative of three independently repeated experiments for the same conditions as in Figure 2 but at a lower concentration of 0.32 μM CdSe/ZnS QD. The peak intensity drops from 127.2 ± 4.4 a.u. in non-irradiated cells to 117.5 ± 4.4 a.u. in irradiated cells. The calculated RPFI is 924 ± 120%. This indicates the profound effect of the presence of QDs before irradiation. The presence of additional ROS produced during and post irradiation caused a statistically significant ($p < 0.001$) optical quenching of 7.6 ± 0.6% in the QD fluorescence intensity. Comparing this result for the 0.32 μM QDs in T98G cells maintained at 1.0 x 10^6 cells/ml, with that for the 0.40 μM QDs in T98G which had a 191.8% increase in the quenching (Figure 2) we speculated that since the amount of QD optical quenching is proportional to the concentration of the ROS in solution [23], then the higher the concentration of QD, the more the production of ROS. To check if this generic conjecture is true in this specific case of QDs and T98G, we measured the fluorescence intensity of T98G cells and QDs at the following final concentrations: 0.2 μM, 0.4 μM, 0.8 μM and 1.6 μM. These concentrations include double (0.8 μM) and quadruple (1.6 μM) of the concentration used in Figure 2. All three repeats (N1, N2 and N3) gave the same results and SI Figure 7 is N1, presented as a representative of all three repeats. The results shown in SI Figure 7 indicate that increased concentrations of QDs at 20 Gy lead to increased fluorescence intensity instead of expected quenching. This suggests a non-linear concentration-response at 20 Gy but leaves intact the ability to compare the effect

Preprints (www.preprints.org) | NOT PEER-REVIEWED | Posted: 28 November 2022 doi:10.20944/preprints202211.0486.v1

of various radiation doses at any specific QD concentration, with the non-irradiated condition as we have done in Figure 2.

3.2. CdSe/ZnS spectroscopy with U87 MG Glioblastoma Cells

Nanoparticle spectroscopy results for U87 MG glioblastoma cells incubated with 0.4 μM core-shell CdSe/ZnS QDs are presented in Figure 3, one of three independent experiments carried out. Here, we varied the radiation dose instead of the concentration of NPs. The fluorescent quenching due to 20 Gy is a lot more than that due to 5 Gy, suggesting that ROS production increases with an increase in radiation dose. Using data plotted in Figure 3, we have a peak intensity of 207.7 ± 1.0 a.u for 5 Gy and 179.8 ± 0.7 a.u for 20 Gy. The difference in the peak intensity for 5 Gy is 3.66 ± 0.01% compared to 16.61 ± 0.01% for 20 Gy with a higher statistical significance (**p<0.01). The calculated RPFI for 5 Gy and 20 Gy are 1677.2 ± 168.0 % and 292.0 ± 29.0 %. The higher RPFI for lower dose could indicate that functionalized nanoparticles have a greater effect at lower doses compared to higher radiation doses.

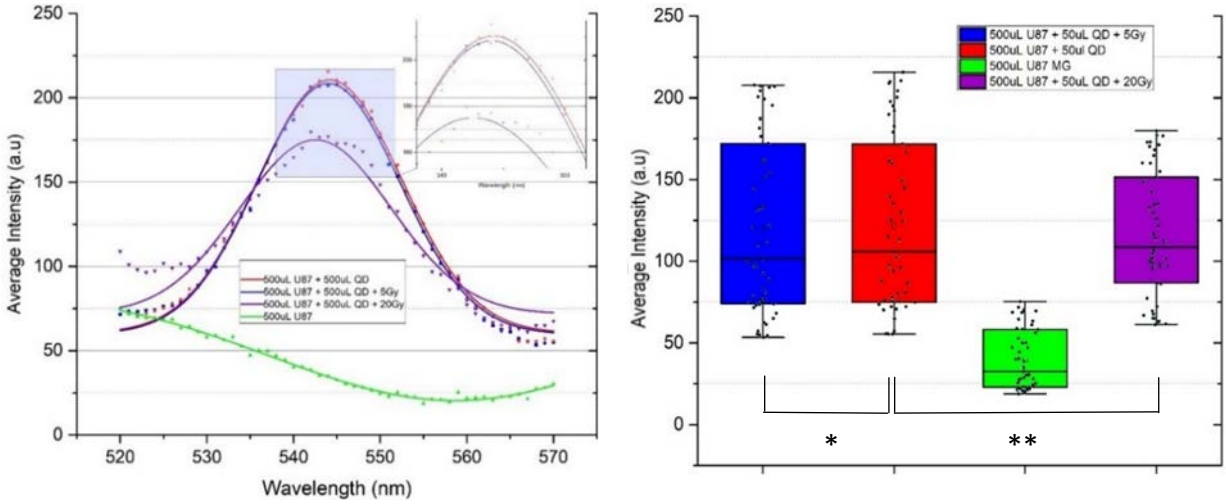

(a) (b)

Figure 3. QD fluorescence spectra and statistical comparisons for U87 MG glioblastoma cells. (a). Average intensity plotted as a function of wavelength. U87 MG cells treated with 0.40 μM core-shell PEGylated CdSe/ZnS QD before 5 Gy and 20 Gy irradiation show reduced intensities. **(b)**. Boxplot showing the range, peak, and mean intensities from Gaussian fits to the raw data of all four conditions in A, f. ANOVA gives statistically significant (**p<0.01 and (*p<0.05) differences in intensities between 20 Gy irradiated (U87 MG+QD+20 Gy), 5 Gy irradiated (U87 MG+QD+5 Gy), and non-irradiated cells (U87 MG+QD), respectively.

However, the dynamic regulation of intracellular and extracellular ROS by cells does engender the need for caution when considering the dose-dependence of any measured changes to NP-induced fluorescence intensities. SI Figure 8 shows the intensity spectra for T98G cells following irradiation at 0.4 μM core-shell PEGylated CdSe/ZnS QD before irradiation at 0, 2, 5, 10, 15, 20 and 50 Gy. There is the expected optical quenching at every dose compared to non-irradiated condition (0 Gy), but the dose-dependence at this QD concentration is non-linear, which might indicate more complex interactions between QDs and irradiation.

3.3. Carbon quantum dot spectroscopy

For carbon quantum dot (CQD) spectroscopy, we did not use PEGylated CQDs as with CdSe/ZnS, owing to the greater biocompatibility of carbon derived NPs, compared with CdSe/ZnS. SI Figure 9 shows the CQD fluorescence spectra and statistical comparisons for T98G glioblastoma cells with conditions including 20 Gy and 5 Gy irradiation following CQD treatment. Interestingly, there is both fluorescence

Preprints (www.preprints.org) | NOT PEER-REVIEWED | Posted: 28 November 2022 doi:10.20944/preprints202211.0486.v1

enhancement and fluorescence quenching of CQD spectra and the occurrence of both enhancement and quenching due to increased ROS production is well known [41-43]. Hence, we quantitatively compare both increase and decrease of fluorescence intensity in terms of percentage changes. Statistical comparisons of the various experimental conditions of T98G cells with CQD showed statistically significant differences ($p<0.01$) between the 20 Gy and 5 Gy irradiated cells and unirradiated cells treated with CQD. In SI Figure 9, the change in the fluorescence intensity due to radiation for CQD in T98G for 20 Gy and 5 Gy are 4.3 ± 0.2% decrease and 18.8 ± 0.2% increase respectively. In another repeat of the experiment, changes in the fluorescence intensity were 15.0 ± 0.2% and 16.1 ± 0.2% for 20 Gy and 5 Gy respectively. In general, there is greater fluorescent enhancement for the 5 Gy compared to the 20 Gy. Furthermore, similar results were obtained with U87 MG glioblastoma cells.

3.4. Impact of NPs on cell migration and cell survival

Our last objective in this work was to find out the therapeutic impact of NP-mediated enhancement of ROS generation in GBM cells during irradiation. More ROS implies more secondary electrons and more secondary electrons implies more local dose deposited [15,18]. Our electrical cell-substrate impedance sensing (ECIS) experiments were done for this purpose. Figure 4 shows typical results for ECIS impedance analysis of CdSe/ZnS functionalized with PEG in U87 MG cell culture medium. The graph shows the influence of PEGylated CdSe/ZnS QD radiosensitizers on U87 MG cell proliferation and migration. The plotted results show that U87 MG cells irradiated without NP radiosensitizers initially migrate more followed by cells incubated with CdSe/ZnS QDs, but after reaching the plateau, the relative pattern of coverage of the electrodes changed.

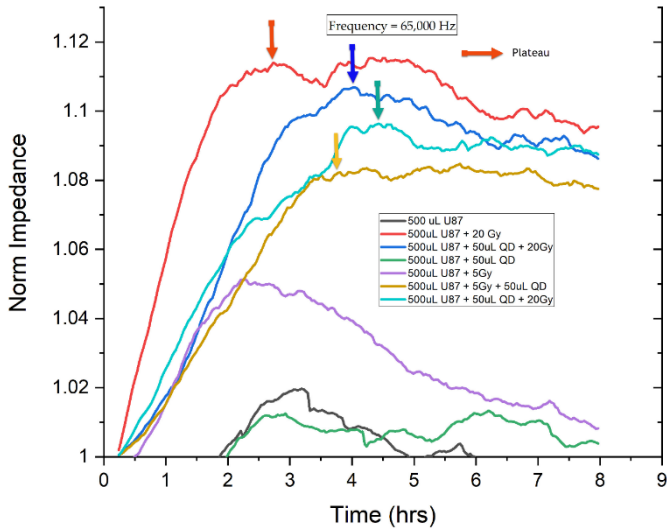

Figure 4. Real-time ECIS monitoring of cell proliferation and migration following NP-based radiosensitization (using CdSe/ZnS QD) and irradiation of U87 glioblastoma cells. U87 cells irradiated without NPs radiosensitizers initially migrate more followed by cells incubated with CdSe/ZnS QDs, but after reaching the plateau, the relative pattern of coverage of the electrodes changed.

The trend shown in Figure 4 is similar for T98G cells incubated with CdSe ZnS QDs where the NPs tend to reduce the initial radiation-induced increase in migration. We also performed ECIS experiments with CQDs for U87 and T98G cells and found similar initial radiation-induced increase in initial migration. Although further analysis of the ECIS results can yield information about putative therapeutic effects of the NPs, we carried out the more classically accepted assessment of the possible radiosensitizing effect of the NPs, using clonogenic assays. The survival curves therefrom are shown in Figure 5 and Figure 6.

Preprints (www.preprints.org) | NOT PEER-REVIEWED | Posted: 28 November 2022 doi:10.20944/preprints202211.0486.v1

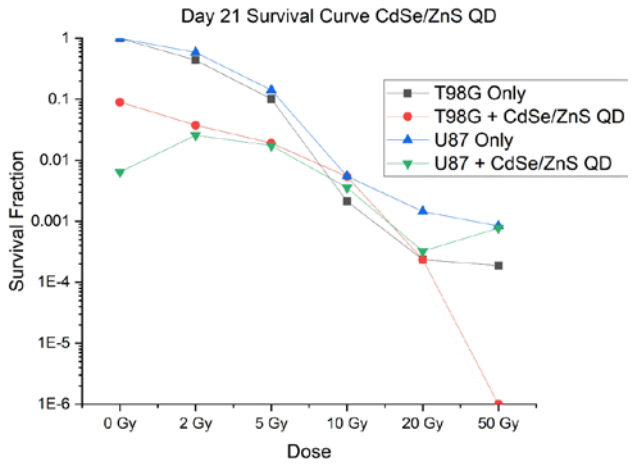

Figure 5. Survival curve for CdSe/ZnS QD. In general, cell survival decreases with increasing dose as expected. T98G cells treated with 0.40 μM CdSe/ZnS QD showed decreased survival compared to T98G only, for most doses especially at 50 Gy. Similarly, U87 cells treated with 0.40 μM CdSe/ZnS QD showed decreased survival compared to U87 only, for most doses especially at 20 Gy. These curves are shown on a semi-log scale and are averages of N1, N2, and N3.

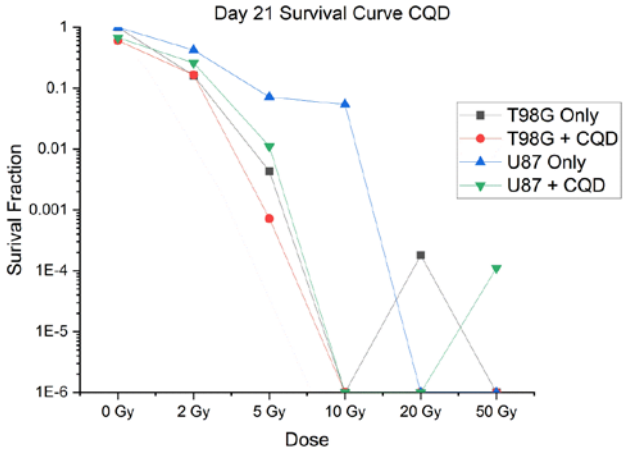

Figure 6. Survival curve for CQD. In general, cell survival decreases with increasing dose as expected. T98G cells treated with 0.2% CQD showed similar survival compared to T98G only, for most doses except at 5 Gy where it CQD treated cells survived less. U87 cells treated with 0.2% CQD showed decreased survival compared to U87 only, for most doses especially at 20 Gy. These curves are shown on a semi-log scale and are averages of N1, N2, and N3.

In Figure 5 where the survival curve for CdSe/ZnS QD is shown, we see the expected pattern of decrease in survival with increasing dose from. The T98G cells treated with CdSe/ZnS QD showed decreased survival compared to T98G only, for most doses especially at 50 Gy ($p<0.001$). Similarly, U87 cells treated with CdSe/ZnS QD showed decreased survival compared to U87 only, for most doses especially at 20 Gy ($p<0.001$). Figure 6 shows the survival curve for CQD. Here, cell survival also decreases with increasing dose as expected. The T98G cells treated with CQD showed similar survival compared to T98G only, for most doses except at 5 Gy where the CQD treated cells survived less ($p<0.001$). U87 cells treated with CQD showed decreased survival compared to U87 only, for most doses especially at 20 Gy ($p<0.01$). These dose-dependent improved cell-killing with NP conditions suggest that future clinically relevant fractionation schemes can be applied and the NER calculated, in view of clinical translation.

 doi:10.20944/preprints202211.0486.v1

4. Discussion

Several other techniques are currently being used to optimize the response of cancer to radiation including dose fractionization in image guided radiotherapy, intensity modulated radiotherapy and volumetric modulated arc therapy, designed to minimize toxicity to healthy tissues, high dose and high dose rate in stereotactic body radiation therapy [44] and systematic administration of radioprotective drugs [45]. A major advantage of the method of using nanoparticles as radiosensitizers [11] in order to improve RT outcomes is that it can be combined with these aforementioned techniques.

An important advantage of our work is the combination of two clonogenic assays, to confirm the efficacy of our chosen NPs as radiosensitizers. We deployed cutting-edge real-time and automated devices, namely, the ECIS for migration and the CytoSMART Omni for clonogenics, to perform these radiosensitization experiments. The real time nature of the impedance readout from ECIS and the real-time/cloud-based live-cell imaging of the CytoSMART Omni permit further end point cell survival assays.

One minor drawback of our work is the generic detection of both intracellular and extracellular ROS. Our probe is not designed to reveal exact ROS species but mainly to pick up interactions between ROS and NPs. Based on our previous work [23,24] and those of others [20-22], the ROS-NP interactions underlying our ROS detection probe includes endogenous hydrogen peroxide, H_2O_2 (which we demonstrated explicitly [23,24]), diffusing across the NP polymer coating layer, leading to chemical oxidation of sulphur or selenium atoms on the CdSe/ZnS QD surface [46]. Interactions of this nature have recently been employed in analytic chemistry for biological applications [47] and help elucidate some of the mechanisms behind our ROS detection assay. Future work will be useful in exploring specific endogenous and exogenous ROS interactions to further optimize NPs for radiosensitization. Notably, both fluorescence quenching (as with CdSe ZnS QDs in this work) and fluorescence enhancement (as with our CQD results) have been found to be readouts of NP-induced ROS generation. It is not surprising that increased ROS generation following irradiation of CQD-incubated GBM cells show up as fluorescence enhancement since both fluorescence enhancement and quenching are known to follow from the interaction of generated ROS depending on interactions at the surface of the QDs or CQDs: increasing electron-withdrawing groups versus increasing electron accepting groups [41-43].

Succinctly, we have shown that biocompatible quantum dots and carbon quantum dots can be used to simultaneously assess ROS generation and radiosensitize glioblastoma cancer cells for possibly improved radiotherapy outcomes.

5. Conclusion

We have demonstrated and confirmed the hypothesis that functionalized, high electron density quantum dots and carbon quantum dots in the presence of radiation amplify the local dose in and around the cells due to an increase in the release of secondary electrons, enhance the generation of reactive oxygen species as a result and consequently, radiosensitize the cancer cells. Thus, we have successfully demonstrated simultaneous assessment of reactive species and radiosensitization of brain cancer cells *in vitro*, using nanoparticle spectroscopy. *In vivo* trials in animal models and *ex vivo* trials using patient samples from diagnostic biopsies are among the next lines of research engendered by our novel approach and findings.

Supplementary Materials: The following are available online at www.mdpi.com/xxx/s1, **Figure S1**: Faxitron CellRad, **Figure S2**: Cell Culture Preparation, **Figure S3**: Full Experimental Workflow, **Figure S4**: How ECIS Works, **Figure S5**: ECIS Results: illustration of impedance as a function of time, **Figure S6**: QD fluorescence spectra and statistical comparisons for T98G glioblastoma cells, **Figure S7:** QD fluorescence spectra at various QD concentrations for T98G glioblastoma cells, **Figure S8:** QD Spectra for T98G cells following irradiation at various doses, **Figure S9:** Carbon QD fluorescence spectra and statistical comparisons for T98G glioblastoma cells.

Author Contributions: Conceptualization, A.E.; methodology, A.E.; software, A.E. and H.D.; formal analysis, H.D., H.K., C.T., Y.W and A.H; investigation, H.D., H.K., C.T., A.H., Y.W., M.M., M.J.M., C.W., H. A., M.J., G.K., A.A., J.B.; resources, A.E.; data curation, A.E., H.D., C.T., Y.W., A.H.; writing—original draft preparation, A.E., H.D., C.T; writing—review and editing, A.E.; visualization, H.D., C.T., Y.W., A.H.; supervision, A.E.; project administration, A.E.; funding acquisition, A.E., C.T., A.H. All authors have read and agreed to the published version of the manuscript.

Funding: This research was funded by Creighton University Startup Grant (240133-215000 FY19) to A.E.

Institutional Review Board Statement: Not applicable.

Informed Consent Statement: Not applicable.

Data Availability Statement: The data that support the findings of this study are available from the corresponding author upon reasonable request.

Acknowledgments: Authors wish to thank all members of the Translational Biomedical Physics Research Group at Creighton University. We also thank Dr Michael Nichols and Dr Andrew Baruth for sharing some lab equipment and supplies with us.

Conflicts of Interest: The authors declare no conflict of interest. The funders had no role in the design of the study; in the collection, analyses, or interpretation of data; in the writing of the manuscript, or in the decision to publish the results.

References

1. Wild, C. P., Weiderpass, E. & Stewart, B. W. *World Cancer report 2020: Cancer Research for Cancer Precention*. *Cancer Control* **199**, (2020).
2. Quick Brain Tumor Facts | National Brain Tumor Society.
3. Dhermain, F. Radiotherapy of high-grade gliomas: current standards and new concepts, innovations in imaging and radiotherapy, and new therapeutic approaches. *Chin. J. Cancer* **33**, 16–24 (2014).
4. Holland, E. C. Glioblastoma multiforme: The terminator. *Proceedings of the National Academy of Sciences of the United States of America* **97**, 6242–6244 (2000).
5. Mehta, M., Khan, A., Danish, S., Haffty, B. G. & Sabaawy, H. E. Radiosensitization of primary human Glioblastoma stem-like cells with low-dose AKT inhibition. *Mol. Cancer Ther.* **14**, 1171–1180 (2015).
6. Grosu, A. L. *et al.* Reirradiation of recurrent high-grade gliomas using amino acid PET (SPECT)/CT/MRI image fusion to determine gross tumor volume for stereotactic fractionated radiotherapy. *Int. J. Radiat. Oncol. Biol. Phys.* **63**, 511–519 (2005).
7. Wernicke, A. G., Smith, A. W., Taube, S. & Mehta, M. P. Glioblastoma: Radiation treatment margins, how small is large enough? *Practical Radiation Oncology* **6**, 298–305 (2016).
8. Lee, Y. W., Cho, H. J., Lee, W. H. & Sonntag, W. E. Whole brain radiation-induced cognitive impairment: Pathophysiological mechanisms and therapeutic targets. *Biomolecules and Therapeutics* **20**, 357–370 (2012).
9. Lamborn, K. R., Chang, S. M. & Prados, M. D. Prognostic factors for survival of patients with glioblastoma: Recursive partitioning analysis. *Neuro. Oncol.* **6**, 227–235 (2004).
10. Zehri, A. H. *et al.* Neurosurgical confocal endomicroscopy: A review of contrast agents, confocal systems, and future imaging modalities. *Surg. Neurol. Int.* **5**, 60 (2014).
11. Wang, H., Mu, X., He, H. & Zhang, X. D. Cancer Radiosensitizers. *Trends in Pharmacological Sciences* **39**, 24–48 (2018).
12. Boateng, F. & Ngwa, W. Delivery of nanoparticle-based radiosensitizers for radiotherapy applications. *International Journal of Molecular Sciences* **21**, (2020).
13. Su, X. Y., Liu, P. D., Wu, H. & Gu, N. Enhancement of radiosensitization by metal-based nanoparticles in cancer radiation therapy. *Cancer Biology and Medicine* **11**, 86–91 (2014).
14. Ghita, M. *et al.* A mechanistic study of gold nanoparticle radiosensitisation using targeted microbeam irradiation. *Sci. Rep.* **7**, (2017).
15. Howard, D., Sebastian, S., Le, Q. V. C., Thierry, B. & Kempson, I. Chemical mechanisms of nanoparticle radiosensitization and radioprotection: A review of structure-function relationships influencing reactive oxygen species. *International Journal of Molecular Sciences* **21**, (2020).
16. Habiba, K. *et al.* Enhancing Colorectal Cancer Radiation Therapy Efficacy using Silver Nanoprisms Decorated with Graphene as Radiosensitizers. *Sci. Rep.* **9**, 1–9 (2019).

17. Mesbahi, A. A review on gold nanoparticles radiosensitization effect in radiation therapy of cancer. *Reports of Practical Oncology and Radiotherapy* **15**, 176–180 (2010).
18. Butterworth, K. T., McMahon, S. J., Currell, F. J. & Prise, K. M. Physical basis and biological mechanisms of gold nanoparticle radiosensitization. *Nanoscale* **4**, 4830–4838 (2012).
19. Roa, W. *et al.* Gold nanoparticle sensitize radiotherapy of prostate cancer cells by regulation of the cell cycle. *Nanotechnology* (2009). doi:10.1088/0957-4484/20/37/375101
20. Ipe, B. I., Lehnig, M. & Niemeyer, C. M. On the generation of free radical species from quantum dots. *Small* **1**, 706–709 (2005).
21. Cooper, D. R., Dimitrijevic, N. M. & Nadeau, J. L. Photosensitization of CdSe/ZnS QDs and reliability of assays for reactive oxygen species production. *Nanoscale* **2**, 114–121 (2010).
22. Luo, Y. H. *et al.* Cadmium-based quantum dot induced autophagy formation for cell survival via oxidative stress. *Chem. Res. Toxicol.* **26**, 662–673 (2013).
23. Lee, B. H., Suresh, S. & Ekpenyong, A. Fluorescence intensity modulation of CdSe/ZnS quantum dots assesses reactive oxygen species during chemotherapy and radiotherapy for cancer cells. *J. Biophotonics* **12**, e201800172 (2018).
24. Djam, K. H., Lee, B. H., Suresh, S. & Ekpenyong, A. E. Quantum Dots for Assessment of Reactive Oxygen Species Accumulation During Chemotherapy and Radiotherapy. in *Methods in Molecular Biology* **2135**, 293–303 (Humana Press Inc., 2020).
25. Haga, Y. *et al.* The effect of ST2 gene product on anchorage-independent growth of a glioblastoma cell line, T98G. *Eur. J. Biochem.* **270**, 163–170 (2003).
26. Clark, M. J. *et al.* U87MG decoded: The genomic sequence of a cytogenetically aberrant human cancer cell line. *PLoS Genet.* **6**, 1000832 (2010).
27. Merrick M, Mimlitz MJ, Weeder C, Akhter H, Bray A, Walther A, Nwakama C, Bamesberger J, Djam H, Abid K, Ekpenyong A. In vitro radiotherapy and chemotherapy alter migration of brain cancer cells before cell death. *Biochem Biophys Rep*. **27**:101071 (2021).
28. Walter Y, Hubbard A, Benoit A, Jank E, Salas O, Jordan D, Ekpenyong A. Development of In Vitro Assays for Advancing Radioimmunotherapy against Brain Tumors. *Biomedicines*. **10**(8):1796 (2022).
29. Pujalté, I. *et al.* Cytotoxicity and oxidative stress induced by different metallic nanoparticles on human kidney cells. *Part. Fibre Toxicol.* **8**, (2011).
30. Klein, S. *et al.* Oxidized silicon nanoparticles for radiosensitization of cancer and tissue cells. *Biochem. Biophys. Res. Commun.* **434**, 217–222 (2013).
31. Klein, S., Sommer, A., Distel, L. V. R., Neuhuber, W. & Kryschi, C. Superparamagnetic iron oxide nanoparticles as radiosensitizer via enhanced reactive oxygen species formation. *Biochem. Biophys. Res. Commun.* **425**, 393–397 (2012).
32. Gara, P. M. D. *et al.* ROS enhancement by silicon nanoparticles in X-ray irradiated aqueous suspensions and in glioma C6 cells. *J. Nanoparticle Res.* **14**, 1–13 (2012).
33. Townley, H. E., Rapa, E., Wakefield, G. & Dobson, P. J. Nanoparticle augmented radiation treatment decreases cancer cell proliferation. *Nanomedicine Nanotechnology, Biol. Med.* **8**, 526–536 (2012).
34. Cui, F. *et al.* Enhancement of radiotherapy efficacy by nanoparticles in gastric cancer cells. *Cancer Lett.* **346**, 2345–2358 (2014).
35. Giaever, I. & Keese, C. R. Micromotion of mammalian cells measured electrically. *Proc. Natl. Acad. Sci. U. S. A.* **88**, 7896–900 (1991).
36. Wegener, J., Keese, C. R. & Giaever, I. Electric cell-substrate impedance sensing (ECIS) as a noninvasive means to monitor the kinetics of cell spreading to artificial surfaces. *Exp. Cell Res.* **259**, 158–166 (2000).
37. Müller, J., Thirion, C. & Pfaffl, M. W. Electric cell-substrate impedance sensing (ECIS) based real-time measurement of titer dependent cytotoxicity induced by adenoviral vectors in an IPI-2I cell culture model. *Biosens. Bioelectron.* **26**, 2000–2005 (2011).
38. Pradhan, R., Mandal, M., Mitra, A. & Das, S. Monitoring cellular activities of cancer cells using impedance sensing devices. *Sensors Actuators, B Chem.* **193**, 478–483 (2014).
39. Keese, C. R., Wegener, J., Walker, S. R. & Giaever, I. Electrical wound-healing assay for cells in vitro. *Proc. Natl. Acad. Sci. U. S. A.* **101**, 1554–1559 (2004).
40. Chiu, S. P., Batsaikhan, B., Huang, H. M. & Wang, J. Y. Application of Electric Cell-Substrate Impedance Sensing to Investigate the Cytotoxic Effects of Andrographolide on U-87 MG Glioblastoma Cell Migration and Apoptosis. *Sensors (Basel)*. **19**, (2019).
41. Esfandiari, N. *et al.* Effect of carbonization degree of carbon dots on cytotoxicity and photo-induced toxicity to cells. *Heliyon* **5**, e02940 (2019).
42. Gao, L. *et al.* Multiple functionalized carbon quantum dots for targeting glioma and tissue imaging. *Opt. Mater. (Amst).* **75**, 764–769 (2018).
43. Wang, L. *et al.* Full-color fluorescent carbon quantum dots. *Sci. Adv.* **6**, eabb6772 (2020).
44. Moding, E. J., Kastan, M. B. & Kirsch, D. G. Strategies for optimizing the response of cancer and normal tissues to radiation. *Nature Reviews Drug Discovery* **12**, 526–542 (2013).

 doi:10.20944/preprints202211.0486.v1

45. Hosseinimehr, S. J. Trends in the development of radioprotective agents. *Drug Discovery Today* **12**, 794–805 (2007).
46. Mancini, M. C., Kairdolf, B. A., Smith, A. M. & Nie, S. Oxidative quenching and degradation of polymer-encapsulated quantum dots: New insights into the long-term fate and toxicity of nanocrystals in vivo. *J. Am. Chem. Soc.* **130**, 10836–10837 (2008).
47. Speranskaya, E. S., Drozd, D. D., Pidenko, P. S. & Goryacheva, I. Y. Enzyme modulation of quantum dot luminescence: Application in bioanalysis. *TrAC - Trends in Analytical Chemistry* **127**, 115897 (2020).